RESEARCH ARTICLE

Check for updates

Assembling lanthanide–transition metal clusters on TiO$_2$ for photocatalytic nitrogen fixation†

Chao-Long Chen,[a] Hai-Ying Wang,[a] Jun-Ping Li,[a] La-Sheng Long, [iD][a,b] Xiang-Jian Kong [iD] *[a,b] and Lan-Sun Zheng[a,b]

Ammonia synthesis using light with low energy consumption offers an effective solution for energy saving and environmental protection. Herein, an abundant oxygen vacancy photocatalyst was synthesized *via* the integration of lanthanide–transition metal (4f–3d) clusters Ln$_{52}$Ni$_{56}$ on the TiO$_2$ surface. The investigation of photocatalytic nitrogen fixation showed that Ln$_{52}$Ni$_{56}$ not only acts as a tool to improve charge separation but also enriches oxygen vacancies. Multiple synergies resulted in a photocatalytic nitrogen fixation efficiency of up to 800 μmol h^{-1} g^{-1} with the direct utilization of nitrogen and water without any sacrificial agents or co-catalysts. Electron paramagnetic resonance spectroscopy was conducted to investigate the mechanism of oxygen vacancy inactivation and recovery. This study provides a reference for the construction of a photochemical nitrogen fixation catalyst driven by defect engineering.

Introduction

Ammonia is an important raw material for synthetic fertilizers and chemical materials, particularly for agricultural and food production.[1] Currently, the manufacture of ammonia mainly relies on the Haber–Bosch process, which consumes considerable energy.[2–5] Therefore, the development of an efficient and sustainable method to synthesize ammonia, using nitrogen and water at normal temperature and pressure, seems promising. Many photocatalytic materials, such as BiOBr, LDHs, and g-C$_3$N$_4$, have been used since the first reported case of photocatalytic nitrogen fixation using TiO$_2$.[6–9] Different studies have reported that defect engineering is considered a powerful tool for providing multiple active sites and reducing energy activation barriers.[10,11] Oxygen vacancies (OVs) have been extensively studied to construct catalytic sites, improve catalytic performance, and reduction of nitrogen.[12–15] The participation of OVs can enhance the adsorption of substrates and adjust the energy band structure of semiconductors.[16] However, the OVs produced *via* annealing by inert gas protection were unstable when exposed to air. Moreover, the control of the catalyst mor-

phology affected the full utilization of OVs.[17–21] The deactivation mechanism of OVs in photocatalytic nitrogen fixation is still unclear, and the regulation of OVs is very challenging.

TiO$_2$ is regarded as a model catalyst owing to its low cost, non-toxicity, and stable structure.[22,23] Many reports have shown that loading various metal nanoparticles or single atoms on the surface of TiO$_2$ semiconductors can produce abundant OVs and improve charge separation, thus improving photocatalytic performance.[16,18] Compared to polydisperse nanoparticles, metal clusters have a monodisperse size and well-defined crystal structures, which provide an ideal model catalyst for investigating the catalytic reaction mechanism.[24–26] Herein, a Ln$_{52}$Ni$_{56}$/TiO$_2$ composite material with abundant oxygen defects was obtained by loading well-defined heterometallic lanthanide–transition metal (4f–3d) clusters Ln$_{52}$Ni$_{56}$, (Ln = Eu, Pr, Nd, Gd) onto the TiO$_2$ surface. The Ln$_{52}$Ni$_{56}$/TiO$_2$ composite exhibited enhanced photocatalytic nitrogen fixation efficiency of up to 800 μmol h^{-1} g^{-1} under nitrogen and water conditions without any sacrificial agents or co-catalysts. The study of the mechanism suggests that the deactivation in solid–liquid phase reactions is attributed to the decrease in OVs caused by the occupation of reactive oxygen species.

[a]*Collaborative Innovation Center of Chemistry for Energy Materials, State Key Laboratory of Physical Chemistry of Solid Surfaces and Department of Chemistry, College of Chemistry and Chemical Engineering, Xiamen University, Xiamen, 361005, China. E-mail: xjkong@xmu.edu.cn*
[b]*Innovation Laboratory for Sciences and Technologies of Energy Materials of Fujian Province (IKKEM), Xiamen, China*
†Electronic supplementary information (ESI) available: Sample preparation; characterization; including Fig. S1–S31 and Table S1. See DOI: https://doi.org/10.1039/d2qi00628f

Results and discussion

Stable clusters formulated as [Ln$_{52}$Ni$_{56}$(IDA)$_{48}$(OH)$_{154}$(H$_2$O)$_{38}$]·(NO$_3$)$_{18}$ (abbreviated as Ln$_{52}$Ni$_{56}$, Ln = Eu, Pr, Nd, and Gd; iminodiacetic acid (H$_2$IDA)) were obtained as described in our previous work.[27] Ln$_{52}$Ni$_{56}$ cluster molecules were added to reac-

2862 | *Inorg. Chem. Front.*, 2022, **9**, 2862–2868

This journal is © the Partner Organisations 2022

tion solution during the formation of TiO_2 *via in situ* hydrothermal synthesis. $Ln_{52}Ni_{56}$ is a class of cationic cluster with four-shell, nesting doll-like structure.[28] In the outermost layer of the structure, some Ni^{II} ions are coordinated by two aqua ligands. These coordinated waters are easily leaved and form empty coordination sites, forming Ni–O coordination bonds with oxygen atoms on TiO_2 in hydrothermal reaction. In addition, the carboxyl oxygen atom of the IDA ligands outside the clusters can also be connected with Ti^{4+} ions through coordination bonds. Different amounts of $Eu_{52}Ni_{56}$ cluster additives (0, 0.1, 0.2, 0.5, 0.7, and 1 mL of 1 mM $Eu_{52}Ni_{56}$ aqueous solution) are denoted here as TiO_2-blank, $Eu_{52}Ni_{56}/TiO_2$-1, $Eu_{52}Ni_{56}/TiO_2$-2, $Eu_{52}Ni_{56}/TiO_2$-3, $Eu_{52}Ni_{56}/TiO_2$-4, and $Eu_{52}Ni_{56}/TiO_2$-5. As shown in Fig. 1a, powder X-ray diffraction (PXRD) patterns indicate that all diffraction peaks match well with anatase-phase TiO_2 (JCPDS no. 21-1272), and no other phase is formed.[16,18] The diffraction intensity of the (101) peak position is slightly reduced and gradually shifts to a lower angle with the participation of the $Ln_{52}Ni_{56}$ clusters (Fig. S1†). This result confirms the successful loading of clusters into TiO_2 and the increase in lattice constants.[16,29,30]

The Transmission electron microscopy (TEM) profiles of TiO_2-blank and $Eu_{52}Ni_{56}/TiO_2$-3 show uniformly distributed tiny nanoparticles approximately 10 nm in diameter (Fig. 1b and S2a†). The high-resolution TEM (HRTEM) profiles of $Eu_{52}Ni_{56}/TiO_2$-3 show a lattice spacing of 0.357 nm, which corresponds to 0.350 nm of the (101) lattice plane in TiO_2 (Fig. S2c and d†). The increase in lattice spacing further confirms that the successful loading of clusters causes lattice distortion and a left shift of the XRD (101) peak.[29,31] Selected area

electron diffraction (SAED) profiles show that the catalyst mainly exposes (101) crystal planes (Fig. S3†). However, it is difficult to directly define the existence of clusters using HRTEM and high-angle annular dark-field scanning TEM (HAADF-STEM) (Fig. S4†). Scanning electron microscopy (SEM) shows that the catalyst has adequate size uniformity and does not significantly change the size of TiO_2 particles (Fig. 1c and S5†). Elemental energy-dispersive X-ray spectroscopy (EDS) profiles (Fig. 1d–h) suggest that $Eu_{52}Ni_{56}$ is uniformly distributed throughout the catalyst.

The X-ray photoelectron spectroscopy (XPS) of TiO_2 before and after loading shows that binding energies are located at 1155, 1126, and 867 eV in the full spectrum of the $Eu_{52}Ni_{56}/TiO_2$-3 sample (Fig. S6†), which are attributed to Eu and Ni.[32] In the XPS profile of Ti 2p (Fig. 2a), the two typical peaks at 458.7 and 464.5 eV are attributed to Ti $2p_{3/2}$ (Ti^{4+}) and $2p_{1/2}$ (Ti^{4+}), respectively. Notably, when compared to TiO_2-blank, the Ti $2p_{3/2}$ and Ti $2p_{1/2}$ peaks of $Eu_{52}Ni_{56}/TiO_2$-3 are shifted in the positive direction by 0.2 and 0.25 eV, respectively. This shift is attributed to the lattice distortions created by the interaction of TiO_2 and $Eu_{52}Ni_{56}$ clusters.[29,33] This observation confirms the XRD and TEM results, showing the successful loading of clusters. To confirm the presence of OVs, the XPS profile of O 1s was analyzed. As shown in Fig. 2b, the three peaks at 530.1, 513.5, and 532.7 eV are attributed to the three forms of internal lattice oxygen, OVs, and surface hydroxyl groups (OH), respectively.[19] According to the integration of the areas of different samples (Fig. S9 and Table S1†), OV concentrations are in the order of $Eu_{52}Ni_{56}/TiO_2$-3 (25.8%) > $Eu_{52}Ni_{56}/TiO_2$-2 (23.2%) > $Eu_{52}Ni_{56}/TiO_2$-1 (19.9%) > $Eu_{52}Ni_{56}/TiO_2$-4 (19.1%) > TiO_2-blank (18.6%) > $Eu_{52}Ni_{56}/TiO_2$-5 (18.4%). The $Eu_{52}Ni_{56}/TiO_2$-3 sample exhibits the highest OV content.
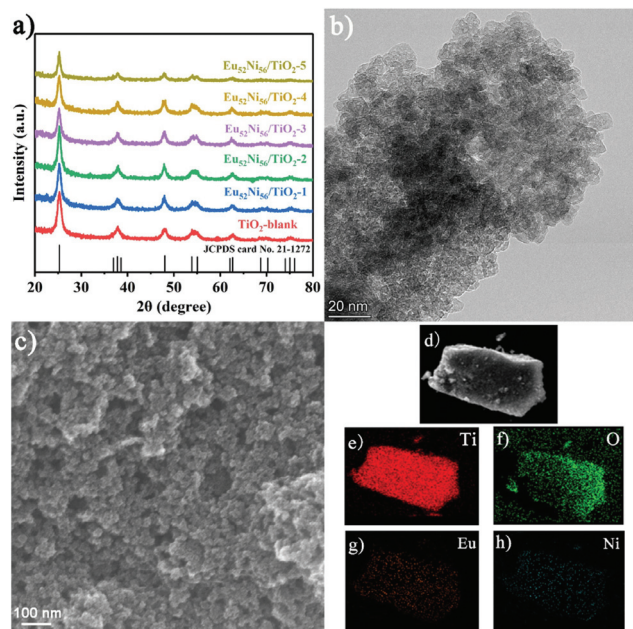

Fig. 1 (a) PXRD patterns of TiO_2-blank and $Eu_{52}Ni_{56}/TiO_2$-1, 2, 3, 4, 5. (b) TEM profile of $Eu_{52}Ni_{56}/TiO_2$-3. (c) SEM profile of $Eu_{52}Ni_{56}/TiO_2$-3. (d–h) Selected area SEM profile of $Eu_{52}Ni_{56}/TiO_2$-3, and corresponding EDX elemental mappings of Ti, O, Eu, and Ni.

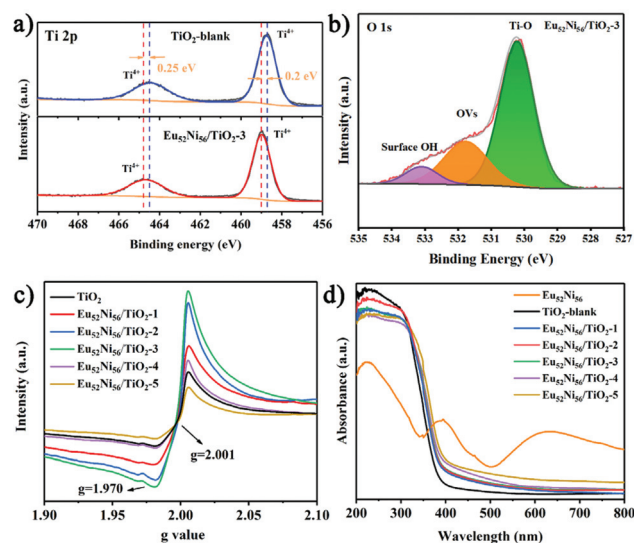Fig. 2 (a) Ti 2p XPS profiles of TiO_2-blank and $Eu_{52}Ni_{56}/TiO_2$-3. (b) O 1s XPS profile of $Eu_{52}Ni_{56}/TiO_2$-3. (c) EPR profiles of TiO_2-blank and $Eu_{52}Ni_{56}/TiO_2$-1, 2, 3, 4, 5. (d) UV-vis DRS profiles of the $Eu_{52}Ni_{56}$ cluster, TiO_2-blank, and $Eu_{52}Ni_{56}/TiO_2$-1, 2, 3, 4, 5.

This journal is © the Partner Organisations 2022

Inorg. Chem. Front., 2022, **9**, 2862–2868 | **2863**

To further confirm the generation of OVs, Electron paramagnetic resonance (EPR) spectroscopy of $Eu_{52}Ni_{56}/TiO_2$ was performed at 110 K without inert gas protection. As shown in Fig. 2c, a particularly distinct EPR peak is observed at a g value of 2.001, which is attributed to the OVs.[19,34] Under the same experimental conditions, $Eu_{52}Ni_{56}/TiO_2$-3 exhibited the highest concentration of OVs, which is consistent with the XPS results. It is worth noting that TiO_2-blank still has a higher OV concentration because of the small and uniform nanoparticles. Based on these results, the loading of $Ln_{52}Ni_{56}$ clusters during *in situ* synthesis can indeed increase the concentration of OVs and have a stabilizing effect. The faint peak at $g = 1.970$ is attributed to Ti^{3+}.[35,36] The UV-vis diffuse reflectance spectroscopy (UV-vis DRS) profiles of the $Eu_{52}Ni_{56}$ cluster, TiO_2-blank, and $Eu_{52}Ni_{56}/TiO_2$-1, 2, 3, 4, 5 are shown in Fig. 2d. TiO_2-blank almost exclusively absorbs ultraviolet light and exhibits only a weak response to visible light because of the charge transfer from the valence band (VB, O 2p orbitals) to the conduction band (CB, Ti 3d orbitals). The measured UV-vis DRS of the $Eu_{52}Ni_{56}$ shows two main peaks of d–d transition for octahedral Ni^{2+} at 400 and 632 nm, which are assigned to $^3A_{2g} \rightarrow {}^3T_{1g}$ (P) and $^3A_{2g} \rightarrow {}^3T_{1g}$ (F), respectively. The absorption of $Eu_{52}Ni_{56}/TiO_2$-1, 2, 3, 4, and 5 improves because of the loading of clusters on TiO_2.[16,18,37] With the increase in $Eu_{52}Ni_{56}$ cluster loading, the apparent color of the catalyst slowly changes from white to yellowish (Fig. S10†), and this corresponds to the increase in light absorption.[38]

Owing to the abundant OVs, the photocatalytic NRR of small catalyst nanoparticles was performed under light irradiation ($\lambda > 300$ nm) using water and N_2 (99.999%) as raw materials without any sacrificial reagents or co-catalysts. The NH_4^+ concentration was detected using Nessler's reagent and ion chromatography methods. As shown in Fig. 3a and S11,† TiO_2-blank exhibits an activity of 228 μmol h^{-1} g^{-1}, which is

attributable to a large number of active OVs that enhance N_2 adsorption and activation.[7,39] As the concentration of OVs increases, the efficiency of $Eu_{52}Ni_{56}/TiO_2$-3 increases to 803 μmol h^{-1} g^{-1}, which is 3.5 times higher than that of TiO_2-blank. The subsequent increase in loading clusters causes a decrease in NRR performance, which is attributed to the large number of clusters covering the active site and reducing the OV concentration.[18] A contrast experiment was performed, under an argon atmosphere, to trace the source of ammonia (Fig. 3b and S12†). When argon was substituted with nitrogen as the feedstock gas, trace activity was observed, which confirmed that N_2 was the origin of NH_3. Another control photocatalytic NRR experiment was conducted with Eu^{3+}, Ni^{2+}, and iminodiacetic acid (H_2IDA). The obtained response was even worse than that of TiO_2-blank (Fig. 3b and S12†), which convincingly illustrated the key role of $Eu_{52}Ni_{56}$ cluster. Five cycles of testing (each run for 1 h, with washing and drying after each run) revealed that $Eu_{52}Ni_{56}/TiO_2$-3 still maintained relatively adequate activity (Fig. 3c), and there was no distinct change in the morphology (Fig. S19 and S20†), indicating high stability. Composite catalysts with different lanthanide elements were studied to compare their performance, since different lanthanide elements may play different roles. Among the isostructural $Ln_{52}Ni_{56}/TiO_2$ series, $Eu_{52}Ni_{56}/TiO_2$ exhibits the best pNRR performance (Fig. 3d), indicating that Eu plays a key role in the entire catalytic system.

Catalytic efficiency gradually decreases during the photocatalytic reaction, and the ammonia yield reaches equilibrium at 5 h (Fig. S13†). Although this phenomenon has been reported in some photocatalytic NRR systems, none of studies discussed the reasons for this decrease in activity. A recent study suggested that a similar phenomenon occurred owing to the occupation of zinc vacancies.[40] To further investigate the mechanism for the decrease in NRR activity and the changes in OV species under light excitation, *in situ* EPR was conducted at 293 K. As shown in Fig. S17 and S18,† the OV signal of the $Eu_{52}Ni_{56}/TiO_2$-3 catalyst shows an obvious decrease after light irradiation. The decrease in OVs is caused by not only N_2 capture but also some oxygen species present at the OV positions. For example, large amounts of water molecules in the reaction can act as competing species for N_2 to occupy the OVs. If the combined water and oxygen species on the catalysts are removed, the OVs may be reexposed and reactivated. Following the NRR reaction, the EPR of the wet sample was performed at 110 K. As shown in Fig. 4a, the EPR spectrum of the wet sample shows a weak signal at $g = 2.001$ after the photoreaction. This suggests that most of the catalyst is deactivated. After drying at 80 °C for 24 h, the EPR results of the deactivated catalyst show enhanced OV signals, indicating that the OVs were restored after drying. The EPR results before and after drying not only illustrate the important role of OVs but also provide strong evidence for the mechanisms of catalyst deactivation and recovery.

To investigate the NRR mechanism of $Eu_{52}Ni_{56}/TiO_2$, photoluminescence spectra were recorded. As shown in Fig. 4b, the emission spectrum of $Eu_{52}Ni_{56}/TiO_2$-3 under excitation at
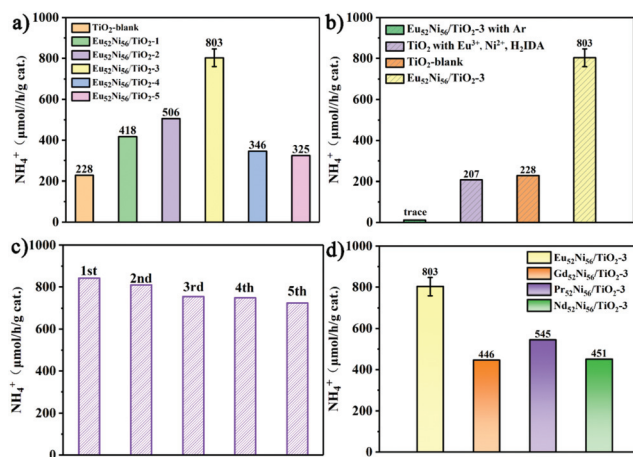

Fig. 3 (a) N_2 reduction activities of TiO_2-blank and $Eu_{52}Ni_{56}/TiO_2$-1, 2, 3, 4, 5. (b) Controlled experiments with TiO_2-blank and $Eu_{52}Ni_{56}/TiO_2$-3. (c) Five catalytic cycles of $Eu_{52}Ni_{56}/TiO_2$-3. (d) N_2 reduction activities of $Eu_{52}Ni_{56}/TiO_2$-3, $Gd_{52}Ni_{56}/TiO_2$-3, $Pr_{52}Ni_{56}/TiO_2$-3, and $Nd_{52}Ni_{56}/TiO_2$-3.

2864 | *Inorg. Chem. Front.*, 2022, **9**, 2862–2868

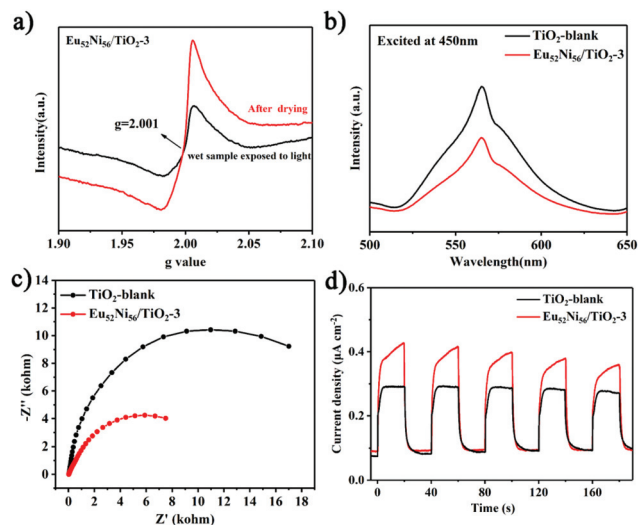This journal is © the Partner Organisations 2022

Fig. 4 (a) EPR spectra of wet $Eu_{52}Ni_{56}/TiO_2$-3 after light irradiation and after drying at 110 K. (b) Photoluminescence spectra of TiO_2-blank and $Eu_{52}Ni_{56}/TiO_2$-3 with excitation at 450 nm. (c) Electrochemical impedance spectroscopy of TiO_2-blank and $Eu_{52}Ni_{56}/TiO_2$-3. (d) Transient photocurrent response of TiO_2-blank and $Eu_{52}Ni_{56}/TiO_2$-3 under simulated irradiation and off.

450 nm exhibits a lower signal than that of TiO_2-blank. This indicates that the recombination of the excited electrons and holes of $Eu_{52}Ni_{56}/TiO_2$-3 is significantly suppressed compared to that of TiO_2-blank. Time-resolved steady state photoluminescence (PL) spectra show that the lifetimes of TiO_2-blank and $Eu_{52}Ni_{56}/TiO_2$-3 are 1.05 and 1.31 ns, respectively (Fig. S21†). The lifetime increase of $Eu_{52}Ni_{56}/TiO_2$-3 indicates an increase in the lifetime of charge carriers.[18,41] Electrochemical impedance spectroscopy (EIS) and transient photocurrent response (TPC) were performed to further investigate the transfer efficiency. As shown in Fig. 4c and d, $Eu_{52}Ni_{56}/TiO_2$-3 has a smaller Nyquist radius and a higher photocurrent response. This confirms that $Eu_{52}Ni_{56}/TiO_2$-3 has a lower interfacial charge transfer resistance and higher electron–hole separation and transfer efficiency compared to those of TiO_2-blank. These results suggest that the rapid charge separation caused by assembling atomically precise clusters on semiconductors is also an important factor in improving photocatalytic performance.[27,42]

Mott–Schottky (MS) analyses show that the CB of $Eu_{52}Ni_{56}/TiO_2$-3 is −0.34 V vs. the normal hydrogen electrode (NHE), which is positive than that of TiO_2-blank (−0.47 V vs. NHE) (Fig. S22 and S23†). The UV-vis diffuse reflectance spectroscopy (UV-DRS) profile shows that the bandgaps for $Eu_{52}Ni_{56}/TiO_2$-3 and TiO_2-blank are 3.08 and 3.20 eV, respectively (Fig. S24†). From calculations, the VB of $Eu_{52}Ni_{56}/TiO_2$-3 and TiO_2-blank are located at 2.74 and 2.73 eV, respectively (Fig. 5 and S25†).[43,44] A narrow band gap can promote the absorption of light energy and improve catalytic activity.[45] According to Mott–Schottky spots and UV-vis DRS of $Ln_{52}Ni_{56}$, the LUMO energy levels of $Eu_{52}Ni_{56}$, $Gd_{52}Ni_{56}$, $Pr_{52}Ni_{56}$, and
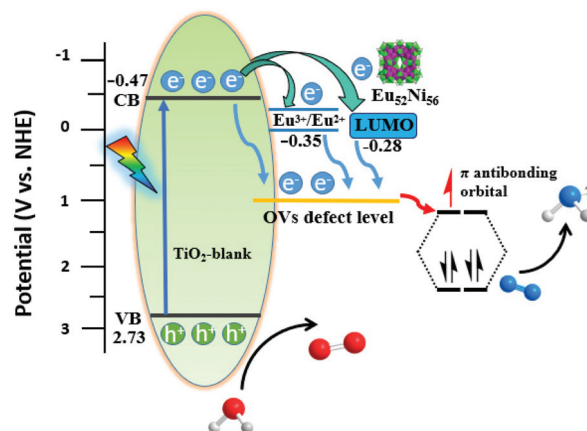

Fig. 5 Charge separation and transfer in the $Eu_{52}Ni_{56}/TiO_2$-3 composite under light irradiation. VB: valence band; CB: conduction band.

$Nd_{52}Ni_{56}$, which are −0.28, −0.26, −0.43, and −0.38 V. vs. NHE, respectively (Fig. S26–29†). Therefore, there is a natural driving force (potential difference) wherein the active electrons in the CB of TiO_2-blank can be transferred to the LUMO energy of $Ln_{52}Ni_{56}$, improving the efficiency of charge separation (Fig. S30†). The energy level of the Eu^{3+}/Eu^{2+}, Nd^{3+}/Nd^{2+}, Gd^{3+}/Gd, and Pr^{3+}/Pr^{2+} reduction potentials are −0.35, −2.7, −2.28 and −3.1 V, respectively.[46,47] The CB of TiO_2-blank (−0.47 V) is negative than the energy level of the Eu^{3+}/Eu^{2+} reduction potential (−0.35 V), indicating that the photoexcited electrons of TiO_2-blank can transfer to Eu^{3+} (Fig. S31a†). However, the energy levels of Nd^{3+}/Nd^{2+}, Gd^{3+}/Gd and Pr^{3+}/Pr^{2+} reduction potentials are more negative than the CB of TiO_2-blank, resulting in the photoexcited electrons of TiO_2-blank cannot transfer to the Nd^{3+}, Pr^{3+} and Gd^{3+} with only migrate to the LUMO energy level of $Nd_{52}Ni_{56}$, $Gd_{52}Ni_{56}$, and $Pr_{52}Ni_{56}$ with a single path (Fig. S31b†). So, the dual-channel charge transfer of $Eu_{52}Ni_{56}/TiO_2$ to Eu^{3+} and LUMO energy level of $Eu_{52}Ni_{56}$ leads to efficient charge separation efficiency and high catalytic activity (Fig. 3d and 5).

Combined with the above analysis, the entire process of the pNRR can be described as follows. Under light irradiation, the photogenerated electrons are quickly transferred to the CB of TiO_2-blank. Most of them recombine with photogenerated cavities, and a small portion is quickly captured by the OV defect.[16] Meanwhile, owing to the well-matched energy levels between TiO_2 and $Eu_{52}Ni_{56}$, some of the electrons in the CB of TiO_2 can be transferred to the LUMO energy level and Eu^{3+} of $Eu_{52}Ni_{56}$, which suppresses the recombination of photogenerated carriers.[48] Because of the lower energy of defect levels, all transferred electrons eventually converge on the OVs that act as trapping sites.[18,49] Subsequently, electrons are injected into the empty anti-bonding orbitals (π^*) of adsorbed N_2, which is accompanied by N≡N triple-bond activation and hydrogenation, resulting in the generation of NH_3.[7,49] The photoinduced holes in the VB of TiO_2-blank, which are oxidation of water into oxygen, and completion of the entire catalytic

process. The $Eu_{52}Ni_{56}$ cluster plays an important synergistic role in improving catalytic activity.

Conclusions

In summary, we reported a method for enhanced photo-catalytic nitrogen fixation by loading atomically precise 4f–3d clusters onto TiO_2 semiconductors. A composite photocatalyst, $Ln_{52}Ni_{56}/TiO_2$, with abundant OVs was prepared using a simple solvothermal method. The investigation of photocatalytic nitrogen fixation showed that $Ln_{52}Ni_{56}$, not only acts as a tool to improve charge separation but also serves as a loading species to increase the number of OVs. $Eu_{52}Ni_{56}/TiO_2$-3 displayed the highest photocatalytic N_2 activity of 800 μmol h^{-1} g^{-1} using nitrogen and water as raw materials without any sacrificial agents or co-catalysts. Notably, this study also revealed the mechanism of catalyst deactivation due to the occupation of OVs by reactive oxygen species in photocatalytic nitrogen fixation. This study suggests a new optimization method for defect and energy bond engineering by assembling atomically precise clusters on the surface of semiconductor materials.

Conflicts of interest

There are no conflicts to declare.

Acknowledgements

Notes and references

1 J. W. Erisman, M. A. Sutton, J. Galloway, Z. Klimont and W. Winiwarter, How a century of ammonia synthesis changed the world, *Nat. Geosci.*, 2008, **1**, 636–639.

2 S. Licht, B. Cui, B. Wang, F.-F. Li, J. Lau and S. Liu, Ammonia synthesis by N_2 and steam electrolysis in molten hydroxide suspensions of nanoscale Fe_2O_3, *Science*, 2014, **345**, 637–640.

3 J. A. Pool, E. Lobkovsky and P. J. Chirik, Hydrogenation and cleavage of dinitrogen to ammonia with a zirconium complex, *Nature*, 2004, **427**, 527–530.

4 J. M. P. Martirez and E. A. Carter, Excited-state N_2 dissociation pathway on Fe-functionalized Au, *J. Am. Chem. Soc.*, 2017, **139**, 4390–4398.

5 C. J. M. van der Ham, M. T. M. Koper and D. G. H. Hetterscheid, Challenges in reduction of dinitrogen by proton and electron transfer, *Chem. Soc. Rev.*, 2014, **43**, 5183–5191.

6 G. Dong, W. Ho and C. Wang, Selective photocatalytic N_2 fixation dependent on g-C_3N_4 induced by nitrogen vacancies, *J. Mater. Chem. A*, 2015, **3**, 23435–23441.

7 H. Li, J. Shang, Z. Ai and L. Z. Zhang, Efficient visible light nitrogen fixation with BiOBr nanosheets of oxygen vacancies on the exposed {001} facets, *J. Am. Chem. Soc.*, 2015, **137**, 6393–6399.

8 G. N. Schrauzer and T. D. Guth, Photolysis of water and photoreduction of nitrogen on titanium dioxide, *J. Am. Chem. Soc.*, 1977, **99**, 7189–7193.

9 Y. F. Zhao, Y. X. Zhao, G. I. N. Waterhouse, L. R. Zheng, X. Z. Cao, F. Teng, L. Z. Wu, C. H. Tung, D. O'Hare and T. R. Zhang, Layered-Double-Hydroxide nanosheets as efficient visible-light-driven photocatalysts for dinitrogen fixation, *Adv. Mater.*, 2017, **29**, 1703828.

10 B. M. Comer, Y.-H. Liu, M. B. Dixit, K. B. Hatzell, Y. Ye, E. J. Crumlin, M. C. Hatzell and A. J. Medford, The role of adventitious carbon in photo-catalytic nitrogen fixation by titania, *J. Am. Chem. Soc.*, 2018, **140**, 15157–15160.

11 H. Li, C. Mao, H. Shang, Z. Yang, Z. Ai and L. Z. Zhang, New opportunities for efficient N_2 fixation by nanosheet photocatalysts, *Nanoscale*, 2018, **10**, 15429–15435.

12 C. Lv, Y. Qian, C. Yan, Y. Ding, Y. Liu, G. Chen and G. Yu, Defect engineering metal-free polymeric carbon nitride electrocatalyst for effective nitrogen fixation under ambient conditions, *Angew. Chem., Int. Ed.*, 2018, **57**, 10246–10250.

13 J. Qian, S. Zhao, W. Dang, Y. Liao, W. Zhang, H. Wang, L. Lv, L. Luo, H.-Y. Jiang and J. Tang, Photocatalytic nitrogen reduction by Ti_3C_2 MXene derived oxygen vacancy-rich C/TiO_2, *Adv. Sustainable Syst.*, 2021, **5**, 2000282.

14 Y. Tong, H. Guo, D. Liu, X. Yan, P. Su, J. Liang, S. Zhou, J. Liu, G. Q. Lu and S. X. Dou, Vacancy engineering of Iron-Doped $W_{18}O_{49}$ nanoreactors for Low-Barrier electrochemical nitrogen reduction, *Angew. Chem., Int. Ed.*, 2020, **59**, 7356–7361.

15 N. Zhang, A. Jalil, D. Wu, S. Chen, Y. Liu, C. Gao, W. Ye, Z. Qi, H. Ju, C. Wang, X. Wu, L. Song, J. Zhu and Y. Xiong, Refining defect states in $W_{18}O_{49}$ by Mo doping: A strategy for tuning N_2 activation towards solar-driven nitrogen Fixation, *J. Am. Chem. Soc.*, 2018, **140**, 9434–9443.

16 J. Li, D. Wang, R. Guan, Y. Zhang, Z. Zhao, H. Zhai and Z. Sun, Vacancy-Enabled mesoporous TiO_2 modulated by nickel doping with enhanced photocatalytic nitrogen fixation performance, *ACS Sustainable Chem. Eng.*, 2020, **8**, 18258–18265.

17 N. Zhang, L. Li, Q. Shao, T. Zhu, X. Huang and X. Xiao, Fe-Doped BiOCl nanosheets with light-switchable oxygen vacancies for photocatalytic nitrogen fixation, *ACS Appl. Energy Mater.*, 2019, **2**, 8394–8398.

18 Y. Zhao, Y. Zhao, R. Shi, B. Wang, G. I. N. Waterhouse, L.-Z. Wu, C.-H. Tung and T. R. Zhang, Tuning oxygen vacancies in ultrathin TiO_2 nanosheets to boost photocatalytic nitrogen fixation up to 700 nm, *Adv. Mater.*, 2019, **31**, 1806482.

19 P. Li, Z. Zhou, Q. Wang, M. Guo, S. Chen, J. Low, R. Long, W. Liu, P. Ding, Y. Wu and Y. J. Xiong, Visible-Light-Driven

2866 | *Inorg. Chem. Front.*, 2022, **9**, 2862–2868

This journal is © the Partner Organisations 2022

nitrogen fixation catalyzed by Bi_5O_7Br nanostructures: Enhanced performance by oxygen vacancies, *J. Am. Chem. Soc.*, 2020, **142**, 12430–12439.

20 J. Yang, Y. Guo, R. Jiang, F. Qin, H. Zhang, W. Lu, J. Wang and J. C. Yu, High-Efficiency "Working-in-Tandem" nitrogen photofixation achieved by assembling plasmonic gold nanocrystals on ultrathin titania nanosheets, *J. Am. Chem. Soc.*, 2018, **140**, 8497–8508.

21 Q. Wu, Q. Zheng and R. van de Krol, Creating oxygen vacancies as a novel strategy to form tetrahedrally co-ordinated Ti^{4+} in Fe/TiO_2 nanoparticles, *J. Phys. Chem. C*, 2012, **116**, 7219–7226.

22 R. Guan, H. Zhai, J. Li, Y. Qi, M. Li, M. Song, Z. Zhao, J. Zhang, D. Wang and H. Tan, Reduced mesoporous TiO_2 with Cu_2S heterojunction and enhanced hydrogen production without noble metal cocatalyst, *Appl. Surf. Sci.*, 2020, **507**, 144772.

23 T. Hisatomi, J. Kubota and K. Domen, Recent advances in semiconductors for photocatalytic and photoelectrochemical water splitting, *Chem. Soc. Rev.*, 2014, **43**, 7520–7535.

24 R. Chen, Z. H. Yan and X. J. Kong, Recent advances in First-Row transition metal clusters for photocatalytic water splitting, *ChemPhotoChem*, 2020, **4**, 157–167.

25 Z.-H. Pan, Z.-Z. Weng, X.-J. Kong, L.-S. Long and L.-S. Zheng, Lanthanide-containing clusters for catalytic water splitting and CO_2 conversion, *Coord. Chem. Rev.*, 2022, **457**, 214419.

26 Z. H. Yan, M. H. Du, J. X. Liu, S. Y. Jin, C. Wang, G. L. Zhuang, X. J. Kong, L. S. Long and L. S. Zheng, Photo-generated dinuclear $\{Eu(II)\}_2$ active sites for selective CO_2 reduction in a photosensitizing metal-organic framework, *Nat. Commun.*, 2018, **9**, 3353.

27 R. Chen, Z. H. Yan, X. J. Kong, L. S. Long and L. S. Zheng, Integration of Lanthanide-Transition-Metal clusters onto CdS surfaces for photocatalytic hydrogen evolution, *Angew. Chem., Int. Ed.*, 2018, **57**, 16796–16800.

28 X. J. Kong, Y. P. Ren, W. X. Chen, L. S. Long, Z. Zheng, R. B. Huang and L. S. Zheng, A four-shell, nesting doll-like 3d–4f cluster containing 108 metal ions, *Angew. Chem., Int. Ed.*, 2008, **47**, 2398–2401.

29 T. Wu, X. Zhu, Z. Xing, S. Mou, C. Li, Y. Qiao, Q. Liu, Y. Luo, X. Shi, Y. Zhang and X. Sun, Greatly improving electrochemical N_2 reduction over TiO_2 nanoparticles by Iron doping, *Angew. Chem., Int. Ed.*, 2019, **58**, 18449–18453.

30 C.-Y. Wang, C. Böttcher, D. W. Bahnemann and J. K. Dohrmann, A comparative study of nanometer sized Fe(iii)-doped TiO_2 photocatalysts: synthesis, characterization and activity, *J. Mater. Chem.*, 2003, **13**, 2322–2329.

31 J. Yang, H. Bai, Y. Guo, H. Zhang, R. Jiang, B. Yang, J. Wang and J. C. Yu, Photodriven disproportionation of nitrogen and its change to reductive nitrogen photofixation, *Angew. Chem., Int. Ed.*, 2021, **60**, 927–936.

32 Z. Yao, F. Jia, S. Tian, C. Li, Z. Jiang and X. Bai, Microporous Ni-Doped TiO_2 film photocatalyst by Plasma electrolytic oxidation, *ACS Appl. Mater. Interfaces*, 2010, **2**, 2617–2622.

33 E. M. Neville, M. J. Mattle, D. Loughrey, B. Rajesh, M. Rahman, J. M. D. MacElroy, J. A. Sullivan and K. R. Thampi, Carbon-Doped TiO_2 and carbon, Tungsten-Codoped TiO_2 through Sol–Gel processes in the presence of melamine borate: Reflections through photocatalysis, *J. Phys. Chem. C*, 2012, **116**, 16511–16521.

34 S. Wang, X. Hai, X. Ding, K. Chang, Y. Xiang, X. Meng, Z. Yang, H. Chen and J. Ye, Light-Switchable oxygen vacancies in ultrafine Bi_5O_7Br nanotubes for boosting solar-driven nitrogen fixation in pure water, *Adv. Mater.*, 2017, **29**, 1701774.

35 Y. Horiuchi, T. Toyao, M. Saito, K. Mochizuki, M. Iwata, H. Higashimura, M. Anpo and M. Matsuoka, Visible-Light-Promoted photocatalytic hydrogen production by using an amino-functionalized Ti(IV) metal–organic framework, *J. Phys. Chem. C*, 2012, **116**, 20848–20853.

36 Z. Li, J.-D. Xiao and H.-L. Jiang, Encapsulating a Co(II) molecular photocatalyst in Metal–Organic Framework for visible-light-driven H^2 Production: Boosting catalytic efficiency via spatial charge separation, *ACS Catal.*, 2016, **6**, 5359–5365.

37 G. Liu, Y. Zhao, C. Sun, F. Li, G. Q. Lu and H.-M. Cheng, Synergistic effects of B/N doping on the visible-light photocatalytic activity of mesoporous TiO_2, *Angew. Chem., Int. Ed.*, 2008, **47**, 4516–4520.

38 G. Colón, M. Maicu, M. C. Hidalgo and J. A. Navío, Cu-doped TiO_2 systems with improved photocatalytic activity, *Appl. Catal., B*, 2006, **67**, 41–51.

39 H. Hirakawa, M. Hashimoto, Y. Shiraishi and T. Hirai, Photocatalytic conversion of nitrogen to ammonia with water on surface oxygen vacancies of titanium dioxide, *J. Am. Chem. Soc.*, 2017, **139**, 10929–10936.

40 H. Han, Y. Yang, J. Liu, X. Zheng, X. Wang, S. Meng, S. Zhang, X. Fu and S. Chen, Effect of Zn vacancies in $Zn_3In_2S_6$ nanosheets on boosting photocatalytic N_2 fixation, *ACS Appl. Energy Mater.*, 2020, **3**, 11275–11284.

41 Y. Bo, H. Wang, Y. Lin, T. Yang, R. Ye, Y. Li, C. Hu, P. Du, Y. Hu, Z. Liu, R. Long, C. Gao, B. Ye, L. Song, X. Wu and Y. J. Xiong, Altering hydrogenation pathways in photocatalytic nitrogen fixation by tuning local electronic structure of oxygen vacancy with dopant, *Angew. Chem., Int. Ed.*, 2021, **60**, 16085–16092.

42 R. Chen, G.-L. Zhuang, Z.-Y. Wang, Y.-J. Gao, Z. Li, C. Wang, Y. Zhou, M.-H. Du, S. Zeng, L.-S. Long, X.-J. Kong and L.-S. Zheng, Integration of bio-inspired lanthanide-transition metal cluster and P-doped carbon nitride for efficient photocatalytic overall water splitting, *Natl. Sci. Rev.*, 2021, **8**, nwaa234.

43 M. K. Nowotny, L. R. Sheppard, T. Bak and J. Nowotny, Defect chemistry of titanium dioxide. Application of defect engineering in processing of TiO_2-Based photocatalysts, *J. Phys. Chem. C*, 2008, **112**, 5275–5300.

44 M. Xing, J. Zhang, F. Chen and B. Tian, An economic method to prepare vacuum activated photocatalysts with high photo-activities and photosensitivities, *Chem. Commun.*, 2011, **47**, 4947–4949.

This journal is © the Partner Organisations 2022

Inorg. Chem. Front., 2022, **9**, 2862–2868 | **2867**

45 X. Chen, N. Li, Z. Kong, W.-J. Ong and X. Zhao, Photocatalytic fixation of nitrogen to ammonia: state-of-the-art advancements and future prospects, *Mater. Horiz.*, 2018, **5**, 9–27.

46 A. J. Bard and L. R. Faulkner, *Electrochemical Methods: Fundamentals and Applications*, 2nd edn, Wiley, 2000.

47 D. R. Lide, G. Baysinger and L. Berger, *CRC Handbook of Chemistry and Physics*, 87th edn, CRC, 2007, p. 1438.

48 L. Shi, Z. Li, L. Ju, A. Carrasco-Pena, N. Orlovskaya, H. Zhou and Y. Yang, Promoting nitrogen photofixation over a periodic WS_2@TiO_2 nanoporous film, *J. Mater. Chem. A*, 2020, **8**, 1059–1065.

49 Y. Li, X. Chen, M. Zhang, Y. Zhu, W. Ren, Z. Mei, M. Gu and F. Pan, Oxygen vacancy-rich MoO_{3-x} nanobelts for photocatalytic N_2 reduction to NH3 in pure water, *Catal. Sci. Technol.*, 2019, **9**, 803–810.

2868 | *Inorg. Chem. Front.*, 2022, **9**, 2862–2868

This journal is © the Partner Organisations 2022